



Study of the Textural Changes in the Nowshera (Pakistan) Ca-Bentonite Caused by the Physical Purification Before and After NaCl Treatment

Liaqat Ali Shah¹ · Muhammad Farooq² · Zait Ullah Shah³ · Francisco Rolando Valenzuela-Díaz⁴

Received: 31 July 2020 / Accepted: 24 November 2020 / Published online: 7 January 2021
© Society for Mining, Metallurgy & Exploration Inc. 2021

Abstract

Bentonite collected from Nowshera (Pakistan) was treated with NaCl, and the $< 2\text{-}\mu\text{m}$ clay fractions were separated by sedimentation process. The textural changes in NaCl treated purified bentonite were compared with raw and physically purified sample. It was detected that the NaCl-treated purified bentonite and the sample purified by simple sedimentation, respectively, consist of sodium-montmorillonite and calcium-montmorillonite as a major clay mineral. The honeycombed-type morphology was observed for both the purified samples; however, the particles of NaCl treated purified bentonite were relatively in a compact form. The particle sizes of both the purified samples were found considerably smaller. The high volume percent of the fine particles was noticed in the NaCl-treated purified bentonite. This attributed that the sodium exchange has a valuable impact on the bentonite dispersion in aqueous media during particle size measurement. The relatively high mesopore area/volume and micropore area/volume and specific surface area (SSA) were detected in purified samples. The NaCl-treated purified sample showed relatively high mesopores area/volume than the sample obtained by simple sedimentation. These changes seem to be originated from either high montmorillonite contents and/or the smaller particle size, which might be produced after the layer rearrangement during the interlayer cation replacement by Na^+ ions. The large SSA and high porosity of purified samples particularly the NaCl-treated bentonite suggest their potential use as adsorbents, catalysts, pharmaceuticals, and cosmetics.

Keywords Clay · Montmorillonite · Porosity · Specific surface area · Sedimentation

1 Introduction

The need to reduce the cost of the industrial sector has led scientists to explore the uses of many low-cost industrial raw materials especially those from natural abundant resources. Among these natural materials, bentonite attracted attention for its large quantity and low costs in addition to its distinctive properties of small particle size, high specific surface area, cation exchange capacity, non-toxicity, and high capacity of

adsorption [1, 2]. These valuable properties make it useful in the fabrication of catalyst beds, papers, clay barriers, cosmetics, bleaching earth, food additives, adsorbents, and pharmaceuticals [3–15]. Bentonite is a geological term primarily consisted of montmorillonite admixed with non-clay minerals as impurities [16]. Bentonite is further classified as sodium bentonite (Na^+ -bentonite) or calcium bentonite (Ca^{2+} -bentonite) on the basis of dominant cations in montmorillonite interlayer being Na^+ or Ca^{2+} . The higher the smectite (i.e., montmorillonite) contents in bentonite, the better the execution of bentonite as a raw material in the industrial sector for its high porous system [4, 5, 17–22]. The following three kinds of pores are the primary sources of the bentonite porosity [23]: macropores (pore width (d) ≥ 50 nm), mesopores ($50 \text{ nm} > d > 2$ nm), and micropores ($d \leq 2$ nm) [24, 25]. These pores are often produced among the following three structural units [20, 26]: layer, particle, and aggregate. Firstly, the layer is the fundamental unit of clay structure. The stacking of layers makes another unit called particle or tactoid. In smectite, the layers are often stacked in particle/tactoid in the turbostratic manner which may contain some of the interlayer pores commonly in the micropore size [20, 27–29]. The micropores

✉ Liaqat Ali Shah
liaqat@uop.edu.pk; drliaqatphy@yahoo.com

¹ Department of Physics, University of Peshawar, Peshawar, KP 25120, Pakistan

² Center of Excellence in Physical Chemistry, University of Peshawar, Peshawar, KP, Pakistan

³ Department of Physics, Kohat University of Science & Technology, Kohat, KP, Pakistan

⁴ Polytechnic School, University of Sao Paulo, Sao Paulo, SP 05508-900, Brazil

produced due to turbostratic piling of smectite layers in tactoid/particle is the acceptable and most satisfactory interpretation [30]. Diffusion between the layers of clay is also a good interpretation for micropores; however, it is only considered for interlayer cations of bulky size such as Cs^+ [30]. Secondly, the particles further combine to build aggregate. The compact of particles within aggregates forms inter-particle pores of mesopore size (less than 40 nm). Finally, aggregates combine to form clusters. The cluster formation from aggregates produces inter-aggregate pores (> 40 nm) [31].

The porous system of bentonite produced from the arrangements of the structural units (i.e., layer, particle, and aggregate) changes with the hydration-dehydration process [32, 33]. The higher the swelling property of bentonite, the more effectively it will perform in a single-layer formation as a separate particle during hydration [34]. The separation of bentonite particles less than 2 μm by sedimentation technique is also an effective process of hydration and dehydration. The different chemical treatments of bentonite before purification by sedimentation can modify the swelling differently [15, 35] and thus modify its textural properties [36]. Bentonites having different composition responses differently to the similar chemical treatment thus affect the purity level, porous system, and size of particle of smectite/bentonite. However, there is a lack of information regarding a comprehensive examination of the NaCl treatment of bentonites having different composition on textural characteristics and also their mutual correlation. Recently, the textural changes of purified Nowshera (Pakistan) bentonite activated with Na_2CO_3 were investigated comprehensively [37]; however, the influence of NaCl treatment/activation on textural characteristics of this bentonite has not been reported yet. Therefore, this research study was intended to examine the changes on the specific surface area, mean pore size, and the pore size analysis of a bentonite by purification before and after NaCl treatment. This study also aimed to examine the influence of NaCl treatment on bentonite dispersion process during particle size measurement by laser diffraction-based particle size instrument, level of purity, and distribution of particle size. The comparison of the obtained results with the existing literature was also the objective of this research, to examine the textural changes originated by NaCl treatment of bentonite having different compositions.

2 Materials and Preparation Methods

2.1 Bentonite Selection

The bentonite from Dag-Ismael Khel (Nowshera district) mines of Pakistan was chosen as a primary sample and labeled as “NRB.” The selected raw bentonite is primarily

consisting of calcium-montmorillonite (Ca^{2+} -montmorillonite) (67.7%), illite (0.32%), albite (17.7%), and quartz (14.3%) [38].

2.2 Preparation of Purified Bentonite Powder

To obtain pure Ca^{2+} -montmorillonite and pure sodium-montmorillonite (Na^+ -montmorillonite), the following procedures were applied as recently described [15].

2.2.1 Method I: Preparation of Pure Ca^{2+} -Bentonite

The schematic diagram for the preparation of pure Ca^{2+} -bentonite is presented in Fig. 1. The dispersion of raw bentonite (5 g) was prepared in 1 L of de-ionized water containing 250 mg of dispersing agent ($\text{Na}(\text{PO}_3)_6$) and kept for 15 h at 25 °C. The clear suspension above the depth of 100 mm was decanted into a clean container. The procedure was repeated three times and finally washed the collected supernatant to remove the $(\text{Na}(\text{PO}_3)_6)$ traces. The sample purified by this technique was marked as “NPB-I.”

2.2.2 Method II: Preparation of Pure Na^+ -Bentonite

To obtain purified Na^+ -bentonite, the following procedure was adopted: Firstly, the NRB sample (60 g) was treated thrice with 1 L of 1 M NaCl aqueous solution and washed with de-ionized water to prepare chloride-free bentonite slurry. Secondly, the sedimentation method was applied as described in method -I but without using a dispersing agent to get purified Na^+ -bentonite. The complete procedure was schematically sketched as demonstrated in Fig. 2. The sample purified by this procedure was marked as “NPB-II.”

2.3 XRD

So as to examine the influence of modification and purification, the X-ray diffraction (XRD) technique was used. The oriented bentonite samples were prepared on glass slides, and their XRD results were recorded by “Siemens D500 diffractometer” with the following parameter: graphite monochromator, $\text{CuK}\alpha$ radiation with generator voltage of 40 kV, and tube current of 40 mA, 2° to 40° 2 θ range, scanning step of 0.02°, and 1 s scanning time per step.

2.4 Particle Size Measurement

The Master-sizer 2000 (“Malvern-Instruments Ltd., Malvern, UK”) was selected for the calculation of particle size of the samples. Each sample in portion was transferred to the dispersing module attached to the analyzer. The studied samples were sonicated before analysis to

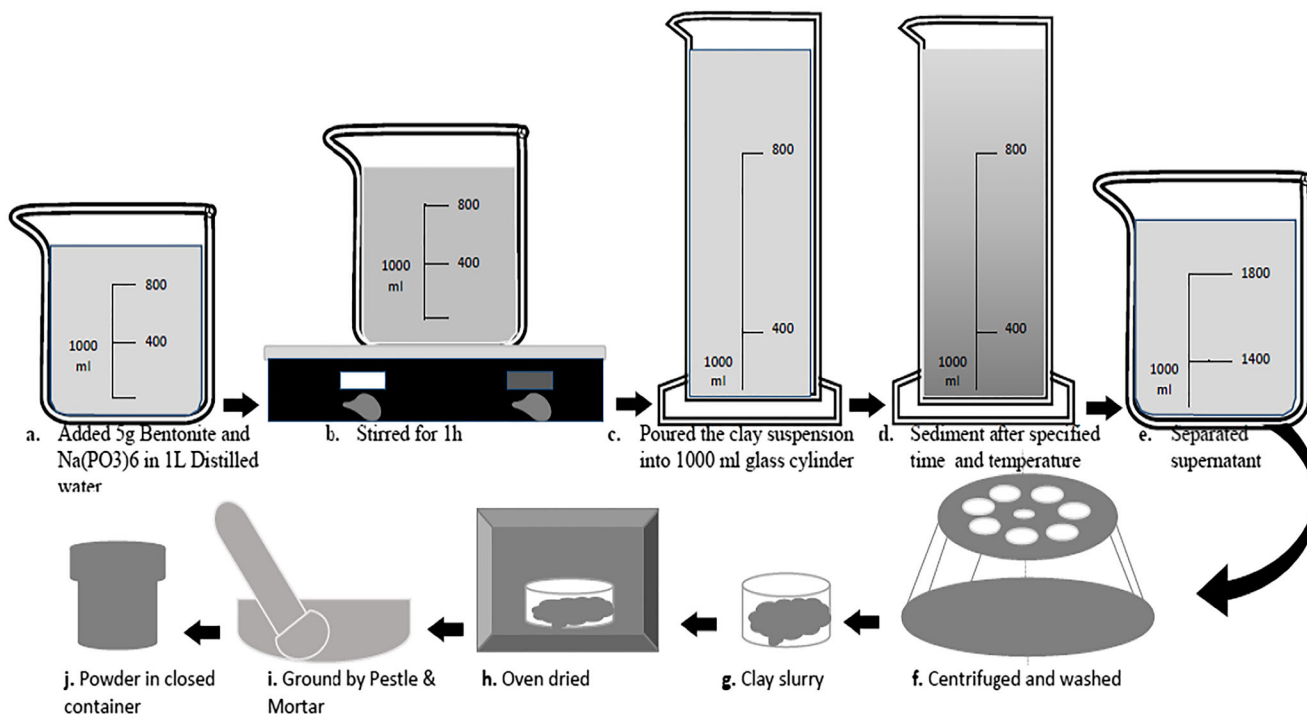


Fig. 1 Schematic diagram for the preparation of pure Ca²⁺-bentonite

properly disperse the sample. The highly dispersed sample was then injected into the analyzer. The size analyses of the sample were measured five times, and their average was recorded as a result.

2.5 PSA and SSA

For specific surface area (SSA) and pore size analysis (PSA), N₂ adsorption-desorption isotherm was recorded by surface area analyzer “Micromeritics ASAP 2010” at 77 K. The PSA was calculated by “Barrett Joyner-Halenda (BJH)” model and SSA by “Brunauer, Emmett, and Teller (BET)”

method. The micropore volume/area was recorded by the t-plot procedure.

2.6 Microstructural Analysis

The morphology of the samples was investigated by a scanning electron microscope (SEM). The powder clay samples were set on the alumina-stub by an adhesive carbon tape and coated with a thin layer of gold. The coated samples were then fixed on the sample holders, and the micrographs needed to analyze the morphology were obtained through a scanning electron microscope (SEM) LEO 440i, equipped with an X-ray energy dispersion spectrophotometer (EDS).

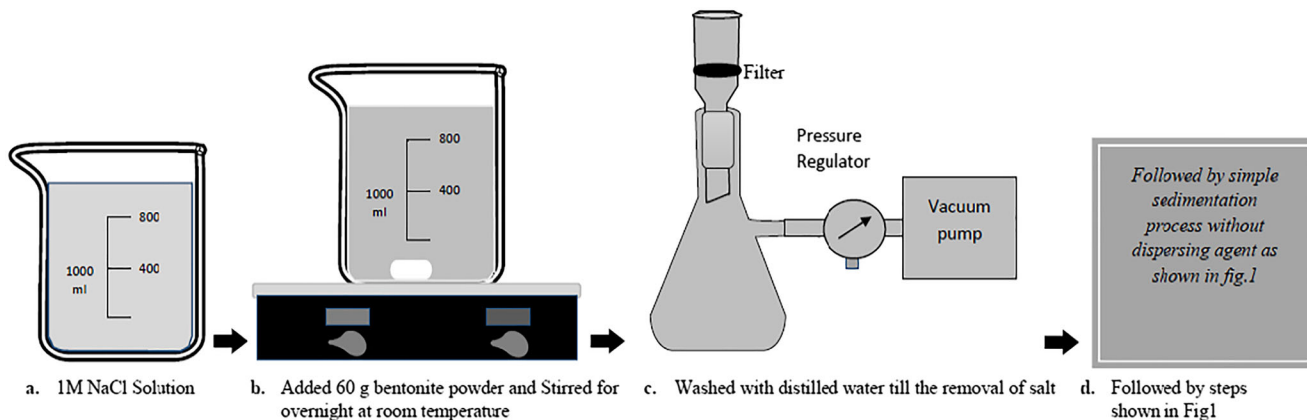


Fig. 2 Schematic diagram for the preparation of pure Na⁺-bentonite

3 Results and Discussion

3.1 X-Ray Diffractograms

The reflection corresponds to d_{001} -value of NRB, NPB-I, and NPB-II denoted by 001_M and 001_I for montmorillonite and illite, respectively (Fig. 3). In the NPB-I and NPB-II samples, the reflections of impurities including quartz were found absent. In NPB-II, the d -value (001_M) was reduced to 12.6 Å (Fig. 3c). This reduction in d -value attributes to Ca^{2+} ion replacement by Na^+ in the montmorillonite interlayer and has been changed into sodium forms. Moreover, the 002 and 004 reflection of montmorillonite appeared while 003 and 005 reflection disappeared indicating the change in orientation of the particle by purification method II.

3.2 Particle Size Measurements

Figure 4 shows the particle size distribution/analysis curves of the studied samples. The volume percent of the submicron particles size was increased drastically by both the purification methods. The NPB-I sample showed maxima at 1.7 μm . The particles larger than 4 μm were found negligible (Fig.4). For the purified sample NPB-II, the size distribution plot displays two maxima: the maxima of smaller volume percentage were centered at 0.23 μm and the maxima of large volume

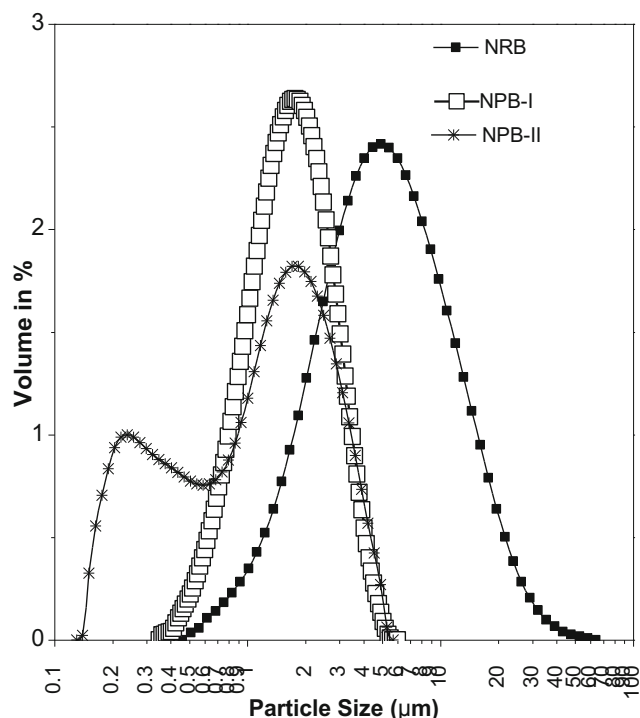
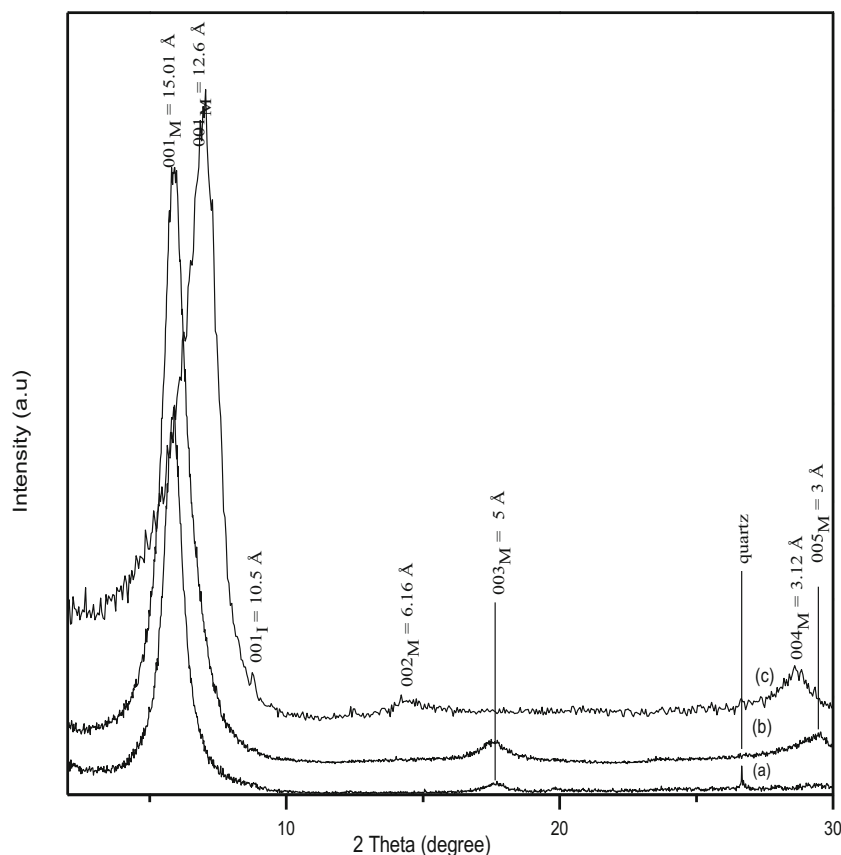


Fig. 4 Particles size distribution for NRB, NPB-I and NPB-II samples

percentage placed at 1.7 μm . This reduction in particle size, in the NPB-II, is the positive effect of Na^+ ion exchange on the

Fig. 3 XRD results of studied samples. **a** NRB. **b** NPB-I. **c** NPB-II. The label 001_M , 002_M , 003_M , 004_M , and 005_M correspond to 001, 002, 003, 004, and 005 reflections of montmorillonite, respectively. The label 001_I corresponds to 001 reflection of illite



bentonite dispersion in aqueous media, during the measurement of particle size by Master-sizer.

A similar behavior regarding particle size changes was also reported for different mineral composition bentonite by purification [36]. The only noticeable difference in particle size distribution curve was as follows: The curve varies in small particle size range before and after the NaCl treatment of the studied bentonite while in bentonite of different composition as studied by Shah and co-workers [36], the curve differs in large particle size range. The Na₂CO₃-activated purified bentonite achieved from the selected/studied bentonite as investigated by Shah [37] comparatively showed particles of large sizes than the currently NaCl-treated purified bentonite. This means the purification of selected bentonite after NaCl treatment is more effective to get smaller-size particles.

3.3 N₂ Adsorption-Desorption Isotherms

In comparison to the “International Union of Pure and Applied Chemistry (IUPAC)” classification of six recommended adsorption isotherm profiles with four different kinds of hysteresis loops [25], the experimental isotherm profiles were identical to type IV and loop of H4 hysteresis (Fig. 5a). The hysteresis part $P/P_0 < 0.45$ and at $P/P_0 = 0.96–1.00$ certified the existence/presence of micro- and macrosize pores, respectively (Fig. 5a).

The hysteresis loops of NPB-I and NPB-II overlapped each other and gave higher volume adsorption than NRB (Fig. 5a).

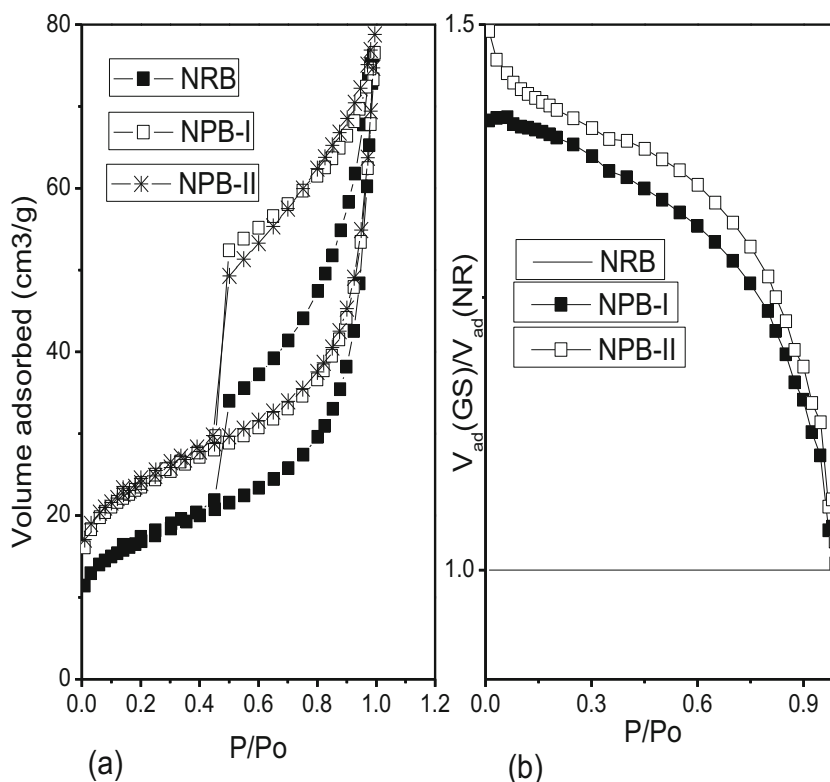
This rise in adsorption volume is the indication of the enhancement in mesopore and micropore volume. The overlapping of isotherms of the NRB, NPB-I, and NPB-II approaching unity showed no significant change in the macropore volume by purification.

3.4 f-Plot Curve/Isotherms

The f-plot isotherms (NRB was selected as a reference) are shown in Fig. 5b. The adsorption ability was increased considerably in NPB-I and NPB-II. For NPB-II, this adsorption increase was noticed comparatively higher especially at low P/P_0 . This difference in adsorption and porosity may be linked either with the total number of layers difference in a particle/tactoid or/and the quantity of montmorillonite contents obtained by purification. Generally, the lesser number of the stacking layers in tactoid/particle creates a large quantity of smaller radii/size pores among the particles and aggregates, and hence high adsorption capacity. Indeed, the f-plot of both the purified samples is not parallel with the x-axis indicating that their surface structure changed noticeably.

These f-plot results are completely different from the recent study of Shah et al. [36]. They claimed that the adsorption performance of the bentonite after purifications by the same two procedures has the same value at low P/P_0 while differ at high P/P_0 . They also claimed that the surface structure has the same behavior as raw sample. Thus, it was concluded that the

Fig. 5 **a** N₂-adsorption-desorption isotherms of NRB, NPB-I, and NPB-II samples. **b** f-plots of NPB-I and NPB-II (reference sample: NRB)



bentonites varying in composition responded differently to the NaCl treatment and purification process.

3.5 SSA

The SSA of the entire studied samples were quantified by the BET procedure using N_2 -adsorption data in the interval $0.05 < x < 0.35$ [39–41]. The SSA values for NRB, NPB-I, and NPB-II were, respectively, 47, 82.4, and 83.5 m^2/g (Table 1). The high percentage increase in SSA is the consequence of the large quantity of smaller diameter pores in NPB-I and NPB-II originated from the high montmorillonite contents obtained by purification.

3.6 Changes in Mesopore Volume/Area

3.6.1 IPV

The incremental pore volume (IPV) of the NRB, NPB-I, and NPB-II showed moderate value at different pore diameter (D) (Fig. 6). Comparing with NPB-I and NPB-II, the IPV for NRB was lower, almost equal, and higher at $D < 6.5$ nm, 6.5 nm $< D < 40$ nm, and $D > 40$ nm, respectively (Fig. 6a). The high value of IPV for NRB at $D > 40$ nm was suggesting the occurrence of greater size inter-aggregate pores. The high pore volume was noticed for NPB-II than for NPB-I. The high IPV for NPB-II was observed until $D < 4.5$ nm. This high IPV value for NPB-II dictated that it contains high quantity of inter-particle pores.

3.6.2 CPV and Mesopore Volume (V_{me})

The intercept of pore size distribution (PSD) curve corresponds to 50 nm of pore diameter valued as the V_{me} (Fig. 6b). The cumulative pore volume (CPV) for NPB-I and NPB-II at $D > 30$ nm and $D < 30$ nm were, respectively, smaller and higher than for the NRB sample (Fig. 6b). The total V_{me} was lowered for NPB-I and NPB-II samples than for the NRB. This variation in V_{me} is the consequence of the pore size difference among the samples.

Table 1 Micropore volume/area, average pore size, and specific surface area of raw and purified samples

Properties	Raw	Purified	
		Method I	Method II
Specific surface area m^2/g	59.08	82.37	83.48
Micropore volume cm^3/g	0.008	0.013	0.014
Micropore area m^2/g	18.58	29.41	32.22
Average pore diameter (nm)	6.30	4.68	4.72

3.6.3 Derivative Mesopore Volume

A large quantity of smaller radii/size pores was found in NPB-I and NPB-II as compared to NRB sample (Fig. 6c). The curve corresponds to NRB sample that showed three maxima, one with a high percentage of mesopore volume positioned at $D \leq 2$ nm, and the others at $D \approx 3$ nm and $D \approx 9$ nm (Fig. 6c). The curves for the NPB-I and NPB-II presented the same nature as NRB; however, the concentration of abundant pores which was increased only at two maxima corresponded to pore of smaller radii. The overlapping maxima of higher value was also noticed for NPB-I and NPB-II at 4 nm $> D > 3$ nm in addition to an increase in dV/dD values at about 3 nm of pore diameter. The individual pore volume corresponds to the first, second, and overlapping maxima for NPB-I and NPB-II contributing highly to the overall pore volume. The pore concentration was found higher for NPB-II at 4 nm $< D < 3$ nm. The large quantity of small size pores in NPB-II sample was indicating that this sample has large quantity of smaller-size particles. These large quantities of smaller size pores in both NPB-I and NPB-II are the primary source of high SSA in these samples.

3.6.4 CPA and Mesopore Area (S_{me})

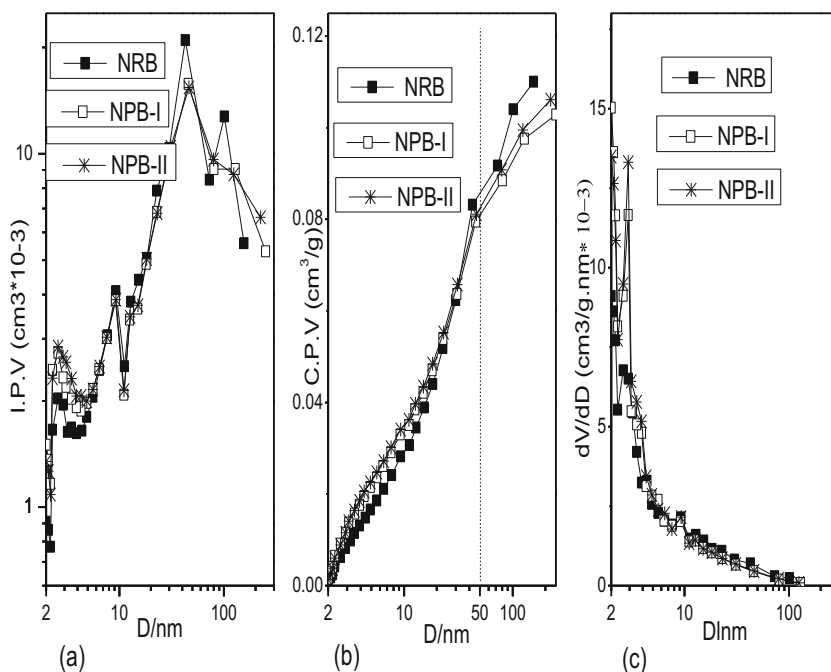
Figure 7a shows the curves of CPA for NRB, NPB-I, and NPB-II. The intercept of the CPA curve at D equal to 50 nm was valued as S_{me} . The S_{me} of both the purified samples was observed higher than NRB; however, the S_{me} of NPB-II was comparatively higher even than of the NPB-I sample as well. Contrary to S_{me} , the V_{me} of NPB-I and NPB-II was relatively lower than that of NRB (Figs. 6b and 7a).

The lower S_{me} for raw sample can be elucidated as follows: Firstly, the mesopore-type pores in NRB might be lowered in numbers than in NPB-I and NPB-II which decrease the total number of pore walls. Secondly, the minerals other than clay such as feldspar and quartz in the NRB sample might affect the layer arrangements inside the particle, particle arrangement inside aggregate, and aggregate in clusters, so, resultantly, the mesoporosity.

3.6.5 Derivative Mesopore Area

The contribution of individual pore area to the total pore area (dA/dD) varied in NRB sample, especially in the 2–4-nm range of pore size (Fig. 7b). The dA/dD maxima at $D \leq 2$ nm and $D \approx 3$ nm were higher for both NPB-I and NPB-II samples than for the NRB sample. In the NPB-I and NPB-II, the overlapping maxima of higher value at 4 nm $< D > 3$ nm were also observed. For NPB-I and NPB-II, the high values of dA/dD correspond to pores of smaller radii, suggesting their higher S_{me} than NRB sample.

Fig. 6 Mesopore volume distributions curves of the NRB, NPB-I, and NPB-II samples. **a** Incremental mesopore volume. **b** Cumulative mesopore volume. **c** Derivative mesopore volume

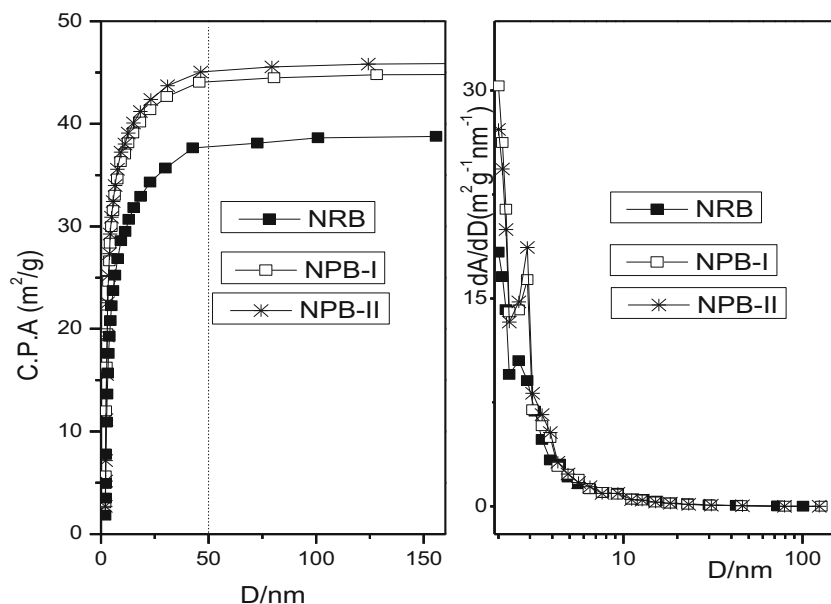


3.7 Changes in Microporosity

The NRB sample was greatly influenced by the purification as the quantity of micropore volume (V_{mic}) and micropore area (S_{mic}) was increased significantly (Table 1). The V_{mic} represents 8% of total pore volume for NRB and increased to 13–14% after purifications (Table 1). The contribution of S_{mic} to the overall pore area was approximately 31% for the NRB sample but increased to 35 and 38%, respectively, for samples NPB-I and NPB-II. The decrease in average pore size from 6

to 4.7 nm was also noticed after purification processes. The smaller mean pore size for the purified sample satisfied the discussion that the NPB-I and NPB-II have a high amount of small-size pores which originates from high montmorillonite contents obtained by purification. In NPB-II, the large number of smaller pores might be the result of the particle/tactoid size reduction after interlayer cation replacement by Na^+ ions which, in succession, play a key role in the formation of a large number of small-size inter-particles and inter-aggregate pores.

Fig. 7 Mesopore area plots of NRB, NPB-I, and NPB-II samples. **a** Cumulative mesopores area. **b** Derivative mesopores area



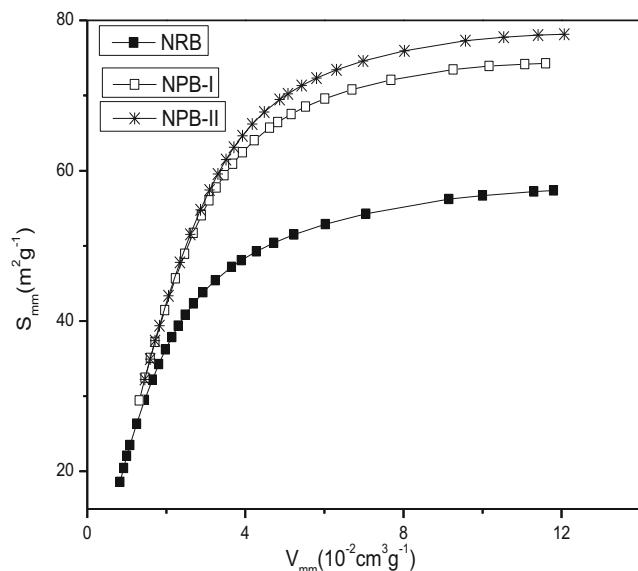


Fig. 8 Micropore-mesopores area vs. micropore-mesopore volume plots of NRB, NPB-I, and NPB-II samples

3.8 Changes in Micro-mesoporosity

The micropore-mesopore volume (V_{mm})/micropore-mesopore area (S_{mm}) was calculated from the mesopore and micropore volume/area combination. In the NRB sample, the S_{mm} first increased sharply and then mildly with the increase of V_{mm} (Fig. 8).

This means, with the continuous increase of mesopores size, the volume of the pore increased uninterruptedly, but

the S_{mm} did not increase linearly as the quantity of wall-splitting pores decreased.

In the NPB-I and NPB-II, the same behavior was achieved; however, the S_{mm} increased significantly with the V_{mm} increase. This prominent increase in purified bentonites can be justified by one or both of the following two reasons: Firstly, a highly pure montmorillonite might be obtained by method-II. Secondly, the particle/tactoid size might be reduced which, resultantly, increase the quantity of mesopores originated from inter-particles and inter-aggregate pores.

3.9 SEM and EDS Results

The SEM results of raw and purified samples are presented in Fig. 9. The raw sample showed moderately planer morphology indicating the dominance in face-to-face interaction between the particles (Fig. 9a). After purification by method I, the structure was completely changed to honeycomb which could be attributed to the edge-face interaction between the particles (Fig. 9b). In comparison with the sample purified by method I, the structure of the raw samples was a little bit coarser because of the presence of impurity contents. In the case of the sample purified by method II, the structure was fairly honeycombed; however, the particles were in more compact form (Fig. 9c). This compact nature shows that the inter particle pores are relatively smaller in the sample purified by method II than those of the original and the sample purified by method I. Moreover, the structural changes in the morphology due to purification methods I and II could also

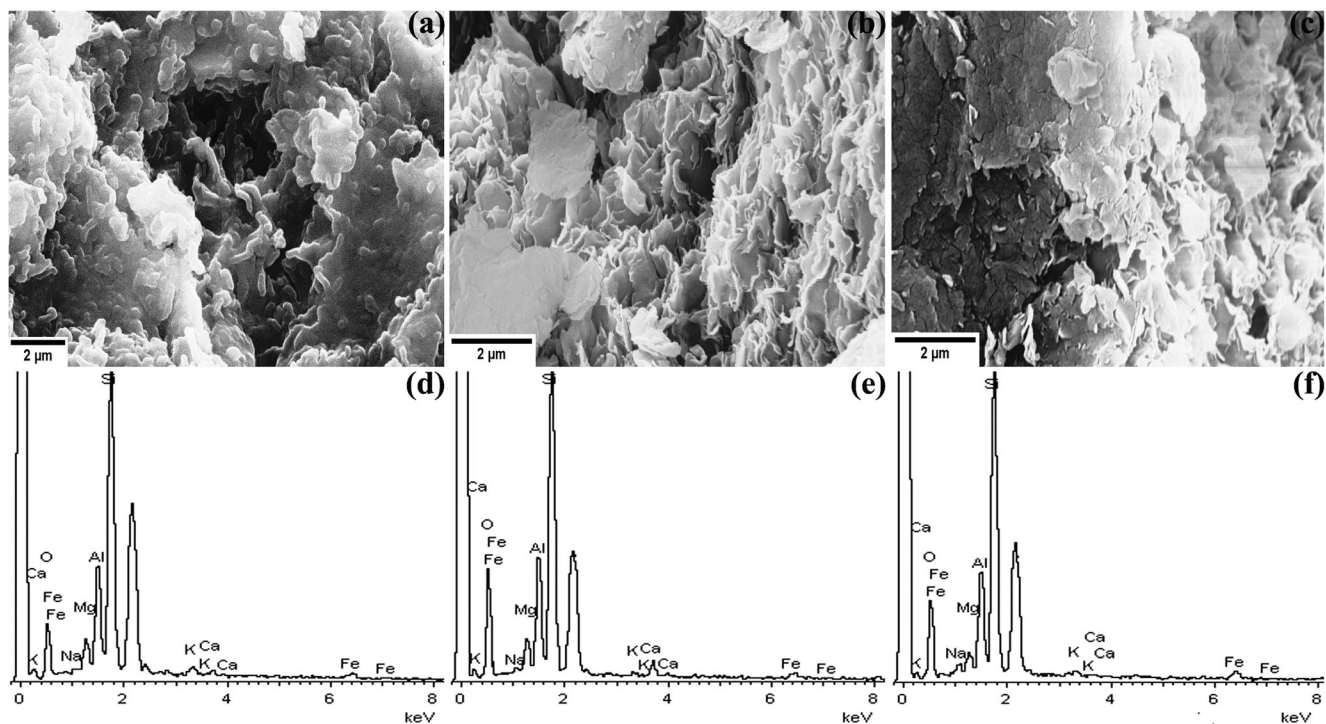


Fig. 9 SEM micrograph and EDS results of the samples. a, d NRB. b, e NPB-I. c, f NPB-II

be linked with the increase in porosity especially mesoporosity as already confirmed from the N_2 desorption-adsorption curves.

The EDS spectrum, presented in Fig. 9d–f, showed the major peaks of Si and Al along with the minor peaks of Ca, Na, K, and Fe in the raw sample which is attributed to the composition of clay minerals. These EDS results are in good conformity with the XRD results (Fig. 1). The EDS spectrum for the sample purified by method I (Fig. 9e) preserved the same shape as for the raw sample (Fig. 9e). However, the peaks of Ca were slightly increased, which could be attributed to the removal of impurities and increasing of the clay mineral contents. In the case of the sample purified by method II, the peaks of Ca and Na were slightly decreased and increased (Fig. 9f), respectively, which can be attributed to the conversion of raw Ca^{2+} -bentonite into Na^+ -bentonite. The observed unlabeled peaks were from gold coating and carbon tape used for SEM.

4 Conclusions

The study of textural modifications in the Ca^{2+} -bentonite caused by purification before and after NaCl treatment was successfully carried out. Based on the results and the above discussion, the following conclusion can be drawn:

- Typically purified Ca^{2+} -bentonite and purified Na^+ -bentonite can be obtained by purification methods I and II, respectively.
- The sample with smaller particle size can be obtained by both the purification methods; however, purification method II could be preferred to obtain large quantity of fine particles.
- The purified Na^+ -bentonites with high capacity of swelling can be achieved by purification method II which performs better information of the smaller-size particle during its hydration in the dispersing module attached with the Master-sizer/particle size-analyzer.
- The microporosity and SSA results for both the purified samples showed approximately similar characteristics. The same effect was also reported for bentonite having different mineral compositions [36]. The currently studied bentonite and the bentonite studied by Shah et al. [36] respond differently to the NaCl treatment and simple sedimentation with respect to surface structure (f-plot method), particle size analyses, and mesoporosity. These differences indicate that bentonites varying in composition respond differently to the different purification processes.
- The similar behavior concerning microporosity attributed that the diffusion of Na^+ cations between the montmorillonite layers has no explicit contribution to bentonite microporosity.

- In the case of V_{me} and S_{me} at smaller size/radii pores, the result for the NPB-I and NPB-II was found different; however, their total pore volume/area was almost equal. These changes can be clarified/explained by any of the following two reasons: First, the sample NPB-II may be composed of high montmorillonite contents. Second, the sample NPB-II may be composed of large quantity of smaller particles which, resultantly, produced pores of smaller radii/size among the particles and aggregates.

Code Availability Not applicable.

Authors' Contributions Not Applicable.

Funding This research work was supported by the Higher Education Commission of Pakistan.

Data Availability Not applicable.

Compliance with Ethical Standards

Conflict of Interest The authors declare that there are no conflicts of interest.

References

1. Abukhadra MR, Seliem MK, Mohamed EA, Selim AQ, Mahmoud MH (2015) Application of quadratic polynomial model for the uptake of iron from aqueous solutions by natural and modified Egyptian bentonite. *Am J Appl Chem* 3:179–183
2. Gamoudi S, Srasra E (2017) Characterization of Tunisian clay suitable for pharmaceutical and cosmetic applications. *Appl Clay Sci* 146:162–166. <https://doi.org/10.1016/j.clay.2017.05.036>
3. Barrer RM (1978) Zeolites and clay minerals as sorbents and molecular sieves. Academic Press, London
4. Carretero MI, Pozo M (2009) Clay and non-clay minerals in the pharmaceutical industry Part I. Excipients and medical applications. *Appl Clay Sci* 46(1):73–80. <https://doi.org/10.1016/j.clay.2009.07.017>
5. Carretero MI, Pozo M (2010) Clay and non-clay minerals in the pharmaceutical and cosmetic industries Part II. Active ingredients. *Appl Clay Sci* 47(3–4):171–181. <https://doi.org/10.1016/j.clay.2009.10.016>
6. Ayari F, Srasra E, Trabelsi-Ayadi M (2005) Characterization of bentonitic clays and their use as adsorbent. *Desalination* 185(1–3):391–397. <https://doi.org/10.1016/j.desal.2005.04.046>
7. Barrer RM (1989) Shape-selective sorbents based on clay-minerals - a review. *Clay Clay Miner* 37(5):385–395. <https://doi.org/10.1346/Cmn.1989.0370501>
8. Lopez-Galindo A, Viseras C, Cerezo P (2007) Compositional, technical and safety specifications of clays to be used as pharmaceutical and cosmetic products. *Appl Clay Sci* 36(1–3):51–63. <https://doi.org/10.1016/j.clay.2006.06.016>
9. Pinnavaia TJ (1983) Intercalated clay catalysts. *Science* 220(4595):365–371. <https://doi.org/10.1126/science.220.4595.365>
10. Srasra E, Bergaya F, Van Damme H, Ariguib NK (1989) Surface properties of an activated bentonite-decolourization of rape-seed oil. *Appl Clay Sci* 4:411–421

11. Takashima M, Sano S, Ohara S (1993) Improved fastness of carbonless paper color images with a new trimethine leuco dye. *J Imaging Sci Technol* 37(2):163–166
12. Dardir FM, Mohamed AS, Abukhadra MR, Ahmed EA, Soliman MF (2018) Cosmetic and pharmaceutical qualifications of Egyptian bentonite and its suitability as drug carrier for praziquantel drug. *Eur J Pharm Sci* 115:320–329. <https://doi.org/10.1016/j.ejps.2018.01.041>
13. Bouazizi A, Saja S, Achiou B, Ouammou M, Calvo JI, Aaddane A, Younsi SA (2016) Elaboration and characterization of a new flat ceramic MF membrane made from natural Moroccan bentonite. Application to treatment of industrial wastewater. *Appl Clay Sci* 132–133:33–40
14. Martinez JM, Volzone C, Garrido LB (2017) Evaluation of polymeric Al-modified bentonite for its potential application as ceramic coating. *Appl Clay Sci* 149:20–27
15. Shah LA, Valenzuela MDD, Ehsan AM, Diaz FRV, Khattak NS (2013) Characterization of Pakistani purified bentonite suitable for possible pharmaceutical application. *Appl Clay Sci* 83–84:50–55. <https://doi.org/10.1016/j.clay.2013.08.007>
16. Shaban M, AbuKhadra MR, Shahien MG, Ibrahim SS (2017) Novel bentonite/zeolite-NaP composite efficiently removes methylene blue and Congo red dyes. *Environ Chem Lett*. <https://doi.org/10.1007/s10311-017-0658-7>
17. de Paiva LB, Morales AR, Diaz FRV (2008) Organoclays: properties, preparation and applications. *Appl Clay Sci* 42(1–2):8–24. <https://doi.org/10.1016/j.clay.2008.02.006>
18. Viseras C, Cerezo P, Sanchez R, Salcedo I, Aguzzi C (2010) Current challenges in clay minerals for drug delivery. *Appl Clay Sci* 48(3):291–295. <https://doi.org/10.1016/j.clay.2010.01.007>
19. Onal M, Sarikaya Y, Alemdaroglu T, Bozdogan I (2002) The effect of acid activation on some physicochemical properties of a bentonite. *Turk J Chem* 26(3):409–416
20. Bergaya F, Theng BKG, Lagaly G (2006) Handbook of clay science. Developments in clay science., vol 1. Elsevier, Amsterdam
21. Grim RE, Güven N (1978) Bentonites : geology, mineralogy, properties and uses. Developments in sedimentology, vol 24. Elsevier Scientific Pub. Co. ; distributors for the United States and Canada, Elsevier/North-Holland, Amsterdam, New York
22. Murray HH (2007) Applied clay mineralogy: occurrences, processing and applications of kaolins, bentonites, palygorskite-sepiolite, and common clays. Elsevier, Oxford
23. Onal M, Sarikaya Y, Alemdaroglu T (2001) Investigation of the microporous and mesoporous structures of the Resadiye (Tokat/Turkey) bentonite and its fractions. *Turk J Chem* 25(2):241–249
24. Fischer C, Gaupp R (2004) Multi-scale rock surface area quantification - a systematic method to evaluate the reactive surface area of rocks. *Chem Erde-Geochem* 64(3):241–256. <https://doi.org/10.1016/j.chemer.2003.12.002>
25. Sing KSW, Everett DH, Haul RAW, Moscou L, Pierotti RA, Rouquerol J, Siemieniowska T (1985) Reporting physisorption data for gas solid systems with special reference to the determination of surface-area and porosity (recommendations 1984). *Pure Appl Chem* 57(4):603–619. <https://doi.org/10.1351/pac198557040603>
26. Touret O, Pons CH, Tessier D, Tardy Y (1990) Study on distribution of water in saturated Mg²⁺ clays with high water-content. *Clay Miner* 25(2):217–233. <https://doi.org/10.1180/claymin.1990.025.2.07>
27. Aylmore LAG, Sills ID, Quirk JP (1970) Surface area of homoionic illite and montmorillonite clay minerals as measured by sorption of nitrogen and carbon dioxide. *Clay Clay Miner* 18(2):91
28. Cases JM, Berend I, Besson G, Francois M, Uriot JP, Thomas F, Poirier JE (1992) Mechanism of adsorption and desorption of water-vapor by homoionic montmorillonite.1. The Sodium-Exchanged Form. *Langmuir* 8(11):2730–2739. <https://doi.org/10.1021/La00047a025>
29. Neaman A, Pelletier M, Villieras F (2003) The effects of exchanged cation, compression, heating and hydration on textural properties of bulk bentonite and its corresponding purified montmorillonite. *Appl Clay Sci* 22(4):153–168. [https://doi.org/10.1016/S0169-1317\(02\)00146-1](https://doi.org/10.1016/S0169-1317(02)00146-1)
30. Michot LJ, Villieras F (2006) Surface area and porosity. In: Bergaya F, Theng BKG, Lagaly G (eds) Handbook of clay science. Elsevier, Amsterdam, pp 965–978
31. Quirk JP, Aylmore LAG (1971) Domains and quasi-crystalline regions in clay systems. *Soil Sci Soc Am Proc* 35(4):652
32. Salles F, Douillard JM, Denoyel R, Bildstein O, Jullien M, Beurroies I, Van Damme H (2009) Hydration sequence of swelling clays: evolutions of specific surface area and hydration energy. *J Colloid Interface Sci* 333(2):510–522. <https://doi.org/10.1016/j.jcis.2009.02.018>
33. Saiyouri N, Hicher PY, Tessier D (2000) Microstructural approach and transfer water modelling in highly compacted unsaturated swelling clays. *Mech Cohesive-Friction Mater* 5(1):41–60. [https://doi.org/10.1002/\(Sici\)1099-1484\(200001\)5:1<41::Aid-Cfm75>3.0.Co;2-N](https://doi.org/10.1002/(Sici)1099-1484(200001)5:1<41::Aid-Cfm75>3.0.Co;2-N)
34. Segad M, Jonsson B, Akesson T, Cabane B (2010) Ca/Na montmorillonite: structure, forces and swelling properties. *Langmuir* 26(8):5782–5790. <https://doi.org/10.1021/la9036293>
35. Shah LA, Khattak NS, Valenzuela MGS, Manan A, Diaz FRV (2013) Preparation and characterization of purified Na-activated bentonite from Karak (Pakistan) for pharmaceutical use. *Clay Miner* 48(4):595–603. <https://doi.org/10.1180/claymin.2013.048.4.03>
36. Shah LA, Valenzuela MDD, Farooq M, Khattak SA, Diaz FRV (2018) Influence of preparation methods on textural properties of purified bentonite. *Appl Clay Sci* 162:155–164
37. Shah LA (2018) Effect of Na₂CO₃ activation and sedimentation on surface area, particle size, and pore size distribution of Pakistani Ca-bentonite. *Arab J Geosci* 11. <https://doi.org/10.1007/s12517-018-3742-9>
38. Shah LA, Farooq M, Carvalho MSF, Silva-Valenzuela MG, Valenzuela-Díaz (2018) Investigation of mineralogy and porosity of two Pakistani bentonites and its corresponding purified bentonites. *Arab J Sci Eng* 43(1):373–382
39. Brunauer S, Emmett PH, Teller E (1938) Adsorption of gases in multimolecular layers. *J Am Chem Soc* 60:309–319. <https://doi.org/10.1021/Ja01269a023>
40. Noyan H, Muserref O, Sarikaya Y (2007) The effect of sulphuric acid activation on the crystallinity, surface area, porosity, surface acidity, and bleaching power of a bentonite. *Food Chem* 105(1):156–163. <https://doi.org/10.1016/j.foodchem.2007.03.060>
41. Sarikaya Y, Ada K, Alemdaroglu T, Bozdogan I (2002) The effect of Al³⁺ concentration on the properties of alumina powders obtained by reaction between aluminium sulphate and urea in boiling aqueous solution. *J Eur Ceram Soc* 22(12):1905–1910. [https://doi.org/10.1016/S0955-2219\(01\)00514-3](https://doi.org/10.1016/S0955-2219(01)00514-3)

Publisher's Note Springer Nature remains neutral with regard to jurisdictional claims in published maps and institutional affiliations.